Wiring Specificity in the Direction-Selectivity Circuit of the Retina

Kevin L. Briggman, PhD[1]; Moritz Helmstaedter, PhD[2]; and Winfried Denk, PhD[2]

[1]National Institute of Neurological Disorders and Stroke
National Institutes of Health
Bethesda, Maryland

[2]Department of Biomedical Optics
Max Planck Institute for Medical Research
Heidelberg, Germany

NOTES

Introduction

The computation of motion direction by direction-selective retinal ganglion cells (DSGCs), discovered almost 50 years ago (Barlow et al., 1964), has defied comprehensive explanation, partly because the wiring diagram of the neuronal circuit underlying this computation is still not known in sufficient detail. DSGCs respond strongly to motion oriented along a preferred direction (PD) but not to null-direction (ND, 180° from the PD) motion. In theory, this asymmetry could arise from increased inhibition during ND motion, increased excitation during PD motion, or a combination of both mechanisms. The asymmetry could be implemented at the structural level or in the wiring of the DS circuitry, or alternatively, could result from unequal synaptic strengths in an otherwise structurally symmetric circuit. Barlow and Levick (1965) favored a mechanism involving the selective preemption of responses during ND motion by lateral inhibition. The magnitude of the inhibitory synaptic input to DSGCs is indeed spatially asymmetric, as patch–clamp recordings from DSGCs have shown (Fried et al., 2002; Taylor and Vaney, 2002). The main source of this inhibition are starburst amacrine cells (SACs): retinal interneurons (Tauchi and Masland, 1984; Famiglietti, 1991) that are necessary in the DS circuit (Yoshida et al., 2001) and release both GABA and acetylcholine (ACh) (O'Malley et al., 1992). SAC dendrites have, furthermore, been shown to be direction-selective, preferring centrifugal motion (Euler et al., 2002).

Attempts to study DS circuit anatomy using light microscopy have led to contradictory results, with some reports (Fried et al., 2002) showing a higher number of neurite proximities from null-side SACs and others not (Famiglietti, 2002; Dong et al., 2004; Chen and Chiao, 2008). Electron microscopy studies of the DS circuit (Famiglietti, 1991; Dacheux et al., 2003) have not, on their part, been able to reconstruct large fractions of SACs and DSGCs in the same piece of tissue.

Serial-section electron microscopy, which was used for the reconstruction of the *Caenorhabditis elegans* nervous system (White et al., 1986), is laborious, uses thicker sections, and its data are occasionally corrupted by sectioning and imaging artifacts. These problems are ameliorated by automating the acquisition of EM data, as in serial block-face electron microscopy (SBEM) (Denk and Horstmann, 2004). SBEM provides the necessary three-dimensional resolution and field of view to follow thin neurites across hundreds of micrometers of complex neuropil.

Functional and Structural Identification of DSGCs

To identify the PDs of ON–OFF DSGCs, we labeled the ganglion cell layer of an adult mouse retina using bulk electroporation (Briggman and Euler, 2011) with the membrane-impermeable form of Oregon Green 488 BAPTA-1, a calcium indicator. This technique prevented the damage that would inevitably result from the pipette penetration needed for AM ester-based loading (Stosiek et al., 2003; Blankenship et al., 2009) and would possibly have resulted from exposing the retina to the detergents used during this procedure. We then used two-photon-excited fluorescence imaging (Denk et al., 1990) to characterize the response properties of GCs while projecting moving-bar stimuli (oriented in eight equally spaced directions) onto the photoreceptors (Euler et al., 2009). We imaged 634 neuronal somata in a 300 × 300 µm region of the ganglion cell layer (GCL) (Fig. 1*b*). Among those were 25 ON–OFF DSGCs with PDs clustering in four groups (Fig. 1*a*). We denoted those groups, which are known to correspond to the cardinal visual axes (Oyster and Barlow, 1967), as northward (N), eastward (E), southward (S), and westward (W). The cells (6

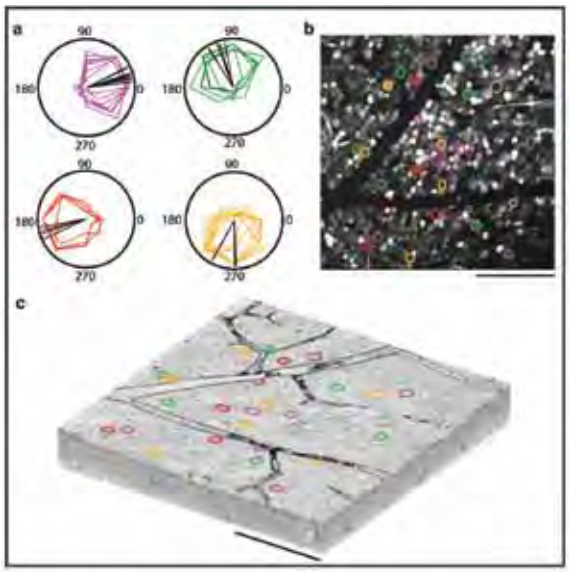

Figure 1. Functional characterization of DSGCs and their localization within the SBEM volume. ***a,*** Polar tuning curves for 25 DSGCs are sorted and color-coded by PD. Black lines indicate the direction of the vector-summed responses. The corresponding soma locations superimposed onto ***b,*** a two-photon image from the recorded region of the ganglion cell layer and ***c,*** the acquired SBEM volume. Note the Y-shaped blood vessel visible in both ***b*** and ***c***. Scale bars, 100 µm.

NOTES

N, 8 E, 7 S, and 4 W) were arranged in a mosaic pattern (Fig. 1*b*). Immediately following two-photon imaging, we fixed and stained the retina and prepared it for SBEM. In order to assist traceability, we specially treated the tissue in order to preferentially label cell surfaces and to leave intracellular structures unstained. The acquired SBEM volume was 350 × 300 × 60 μm^3 in extent, spanned the inner plexiform layer, and contained the GCL and part of the inner nuclear layer. The lateral resolution was 16.5 × 16.5 nm and the section thickness (z-resolution) was 23 nm. All calcium-imaged somata (Fig. 1*c*) were included in the acquired SBEM volume.

Vasculature landmarks were used to identify the somata of the recorded DSGCs in the SBEM volume (Fig. 1*c*). Beginning at their somata, we traced the dendritic trees of 6 DSGCs (Fig. 2*a*; 2 N, 1 E, 1 S, and 2 W cells). Instead of contouring each dendrite, we traced skeletons along the center lines of the dendrites, which speeds up the tracing process considerably (Helmstaedter et al., 2011). The resulting dendritic trees all ramified in two distinct sublayers in the inner plexiform layer (IPL) and overlapped each other horizontally (Fig. 2*a*). The output synapses of SACs are formed at varicosities along the distal third of their dendrites (Famiglietti, 1991) and are geometrically conspicuous, with the presynaptic varicosity wrapping around postsynaptic dendrites (Yamada et al., 2003). We therefore identified such varicose contacts (n = 24 contacts) on both the ON and OFF dendrites of each of the DSGCs and traced the putative presynaptic neurites back to their respective somata. Starting at these somata, we then skeletonized most of their dendritic trees, which substantially overlapped the dendritic fields of the DSGCs (Fig. 2*b*). In every instance, the back-traced cell was a SAC, recognizable by its radially symmetric morphology and costratification with either ON or OFF DSGC arbors (n = 11 ON, 13 OFF SACs). Given an estimated SAC density (including ON and OFF SACs) of 2000/mm^2 for the mouse (Keeley et al., 2007), we skeletonized 11% of all SAC somata in the dataset.

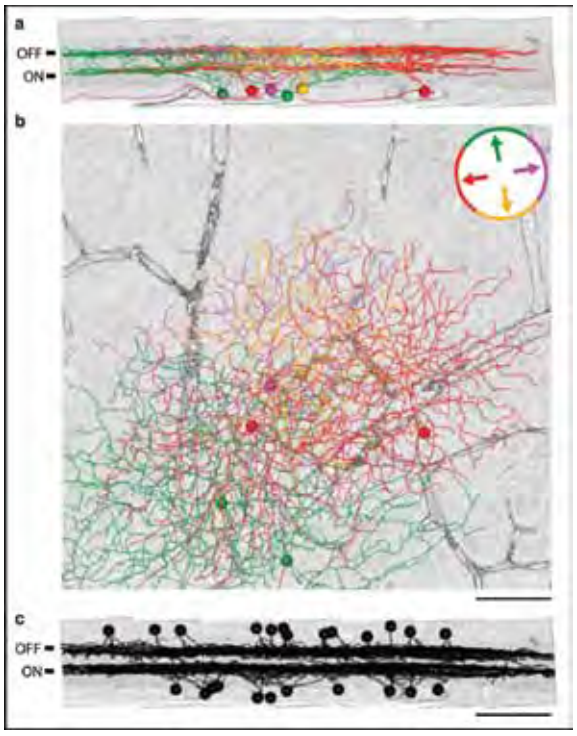

Figure 2. Skeleton reconstructions of DSGCs and SACs. DSGCs, color-coded by PD (inset), projected parallel to ***a*** and normal to ***b*** the plane of the retina. Note bistratification in the IPL. Parallel projections (***c***) of 24 SACs (11 ON SACs, 13 OFF SACs, black). Scale bars, 50 μm.

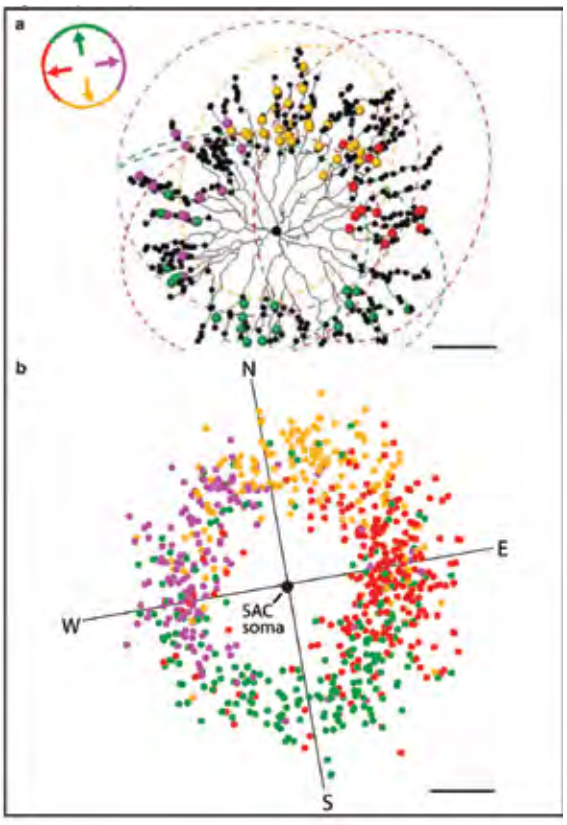

Figure 3. Specificity of SAC outputs. ***a,*** An OFF SAC (black skeleton), with varicosities indicated by black dots. DSGC dendritic trees indicated by color-coded dashed ellipses. Synapses are color-coded by the PD of the postsynaptic DSGC. ***b,*** Output synapse locations (n = 831 synapses) relative to SAC somata from all 24 SACs. Scale bars, 50 μm.

NOTES

Synaptic Connections Between SACs and DSGCs

To identify all additional potential contacts between the 24 SACs and 6 DSGCs that were reconstructed, we next inspected all locations where a SAC and a DSGC skeleton came within 1.5 µm of each other. Of 9260 such locations, 831 were varicose contacts and were marked as putative synapses.

We first examined the specificity of SAC/DSGC synapses from the perspective of individual SACs. We chose one OFF and one ON SAC (Fig. 3*a*) that each overlapped with the 6 DSGCs and color-coded their output synapses by the PDs of the respective DSGCs (Fig. 3*b*; purple: E, green: N, red: W, orange: S). In addition, we identified all the remaining varicosities on the dendrites of these two SACs (413, ON SAC; 452 OFF SAC; black dots in Fig. 3*a*). Output synapses preferred DSGCs with a PD antiparallel to the SAC dendrite (and hence aligned with the ND). For example, the northward-oriented branches of the SACs mostly synapsed onto the southward-preferring (orange) DSGC. Despite a large overlap of these northward branches with the dendritic trees of westward (red) and eastward (purple) DSGCs (Fig. 3*a*), the northward branches avoided synapsing onto them. The specificity is even more apparent in the outputs to the two westward (red) DSGCs. This pattern of specificity was found across all reconstructed SACs (Fig. 3*b*). A given SAC branch does not exclusively synapse onto only one type of DSGC; instead, synapses onto DSGCs with different PDs sometimes occur, in particular for dendrites oriented in between the cardinal directions. We observed no obvious difference in the selectivity between ON and OFF sublayers (data not shown).

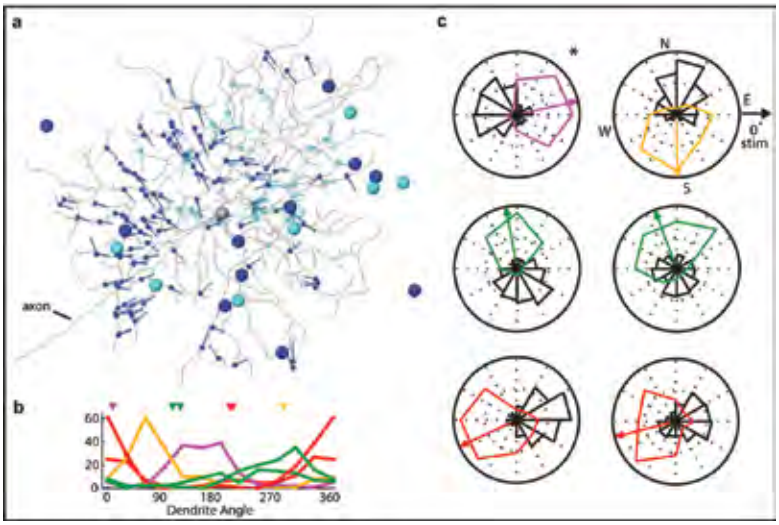

Figure 4. Specificity of DSGCs inputs. ***a,*** DSGC (gray skeleton) and the connected ON and OFF SAC somata (large cyan and blue circles, respectively) and associated SAC input synapses (smaller cyan and blue circles) from 18 SACs. ***b,*** The distribution of all SAC dendrite angles (θ_{dendr}) for each of the 6 DSGCs; θ_{dendr} is defined by the vectors (cyan and blue lines in (***a***) oriented from SAC somata to synapse location. Triangle markers indicate the PD for each DSGC. ***c,*** Polar histograms of θ_{dendr} (black, plotted as the square root of θ_{dendr} frequencies) together with the DSGC tuning curves (as in **Fig. 1**). Asterisk denotes the DSGC shown in ***a.***

We next examined the specificity of synapses from the perspective of individual DSGCs. For each SAC/DSGC synapse, we constructed a vector oriented from its presynaptic SAC soma to the synapse location (Fig. 4*a*). We measured the (dendrite) angle between this vector and the 0° stimulus direction. The distribution of dendrite angles was strongly nonuniform for each DSGC (Fig. 4*b*), with the majority of SAC dendrites oriented opposite to the DSGC's preferred direction (Fig. 4*c*). The difference between dendrite angle and PD was 165.2° ± 51.7° (mean ± SD; $n = 831$).

Discussion

Our data show that SAC dendrites selectively synapse with a DSGC if they are oriented along its ND. This pattern provides the structural substrate for the functional asymmetry in the inhibitory input currents observed in DSGCs (Fried et al., 2002; Taylor and Vaney, 2002). The wiring specificity is apparent both from the perspective of the SACs' outputs (Fig. 3) and that of the DSGCs' inputs (Fig. 4). Dendritic branches of SACs are individually direction-selective for centrifugal motion (Euler et al., 2002), with several mechanisms likely to contribute to this effect (Lee and Zhou, 2006; Hausselt et al., 2007; Oesch and Taylor, 2010). Our data support the view that DSGCs acquire their direction-selectivity predominately by collecting those SAC inputs that suppress ND excitation, i.e., from branches oriented along the ND. Our data are also consistent with the idea that ND SAC input inhibits the initiation of DSGC dendritic spikes during ND motion (Schachter et al., 2010).

NOTES

The approach we used here — tracing a cell and then going on to trace synaptically connected cells — is a virtual version of transsynaptic-virus tracing (Wickersham et al., 2007; Granstedt et al., 2009). While not yet providing the spatial reach of real virus methods, our approach, unlike those, does reveal the strength of connections in terms of the number of contacts and makes possible an analysis of contact areas when needed. Whereas the current study relied on targeted sparse reconstructions, similar SBEM data can and likely will be used for the dense (connectomic) reconstruction of the complete retinal circuitry.

References

Barlow HB, Levick WR (1965) The mechanism of directionally selective units in rabbit's retina. J Physiol 178:477-504.

Barlow HB, Hill RM, Levick WR (1964) Retinal ganglion cells responding selectively to direction and speed of image motion in the rabbit. J Physiol 173:377-407.

Blankenship AG, Ford KJ, Johnson J, Seal RP, Edwards RH, Copenhagen DR, Feller MB (2009) Synaptic and extrasynaptic factors governing glutamatergic retinal waves. Neuron 62:230-241.

Briggman KL, Euler T (2011) Bulk electroporation and population calcium imaging in the adult mammalian retina. J Neurophysiol 105:2601-2609.

Chen YC, Chiao CC (2008) Symmetric synaptic patterns between starburst amacrine cells and direction selective ganglion cells in the rabbit retina. J Comp Neurol 508:175-183.

Dacheux RF, Chimento MF, Amthor FR (2003) Synaptic input to the on-off directionally selective ganglion cell in the rabbit retina. J Comp Neurol 456:267-278.

Denk W, Horstmann H (2004) Serial block-face scanning electron microscopy to reconstruct three-dimensional tissue nanostructure. PLoS Biol 2:e329.

Denk W, Strickler JH, Webb WW (1990) Two-photon laser scanning fluorescence microscopy. Science 248:73-76.

Dong W, Sun W, Zhang Y, Chen X, He S (2004) Dendritic relationship between starburst amacrine cells and direction-selective ganglion cells in the rabbit retina. J Physiol 556:11-17.

Euler T, Detwiler PB, Denk W (2002) Directionally selective calcium signals in dendrites of starburst amacrine cells. Nature 418:845-852.

Euler T, Hausselt SE, Margolis DJ, Breuninger T, Castell X, Detwiler PB, Denk W (2009) Eyecup scope—optical recordings of light stimulus-evoked fluorescence signals in the retina. Pflugers Arch 457:1393-1414.

Famiglietti EV (1991) Synaptic organization of starburst amacrine cells in rabbit retina: analysis of serial thin sections by electron microscopy and graphic reconstruction. J Comp Neurol 309:40-70.

Famiglietti EV (2002) A structural basis for omnidirectional connections between starburst amacrine cells and directionally selective ganglion cells in rabbit retina, with associated bipolar cells. Vis Neurosci 19:145-162.

Fried SI, Munch TA, Werblin FS (2002) Mechanisms and circuitry underlying directional selectivity in the retina. Nature 420:411-414.

Granstedt AE, Szpara ML, Kuhn B, Wang SS, Enquist LW (2009) Fluorescence-based monitoring of *in vivo* neural activity using a circuit-tracing pseudorabies virus. PLoS One 4:e6923.

Hausselt SE, Euler T, Detwiler PB, Denk W (2007) A dendrite-autonomous mechanism for direction selectivity in retinal starburst amacrine cells. PLoS Biol 5:e185.

Helmstaedter M, Briggman KL, Denk W (2011) High-accuracy neurite tracing for high-throughput neuroanatomy. Nat Neurosci 14:1081-1088.

Keeley PW, Whitney IE, Raven MA, Reese BE (2007) Dendritic spread and functional coverage of starburst amacrine cells. J Comp Neurol 505:539-546.

Lee S, Zhou ZJ (2006) The synaptic mechanism of direction selectivity in distal processes of starburst amacrine cells. Neuron 51:787-799.

Oesch NW, Taylor WR (2010) Tetrodotoxin-resistant sodium channels contribute to directional responses in starburst amacrine cells. PLoS One 5:e12447.

O'Malley DM, Sandell JH, Masland RH (1992) Co-release of acetylcholine and GABA by the starburst amacrine cells. J Neurosci 12:1394-1408.

Oyster CW, Barlow HB (1967) Direction-selective units in rabbit retina: distribution of preferred directions. Science 155:841-842.

Schachter MJ, Oesch N, Smith RG, Taylor WR (2010) Dendritic spikes amplify the synaptic signal to enhance detection of motion in a simulation of the direction-selective ganglion cell. PLoS Comput Biol 6.

Stosiek C, Garaschuk O, Holthoff K, Konnerth A (2003) *In vivo* two-photon calcium imaging of neuronal networks. Proc Natl Acad Sci USA 100:7319-7324.

Tauchi M, Masland RH (1984) The shape and arrangement of the cholinergic neurons in the rabbit retina. Proc R Soc Lond B Biol Sci 223:101-119.

Taylor WR, Vaney DI (2002) Diverse synaptic mechanisms generate direction selectivity in the rabbit retina. J Neurosci 22:7712-7720.

White JG, Southgate E, Thomson JN, Brenner S (1986) The structure of the nervous system of the nematode *Caenorhabditis elegans*. Philos Trans R Soc Lond A 314:1-340.

Wickersham IR, Finke S, Conzelmann KK, Callaway EM (2007) Retrograde neuronal tracing with a deletion-mutant rabies virus. Nat Methods 4:47-49.

Yamada ES, Dmitrieva N, Keyser KT, Lindstrom JM, Hersh LB, Marshak DW (2003) Synaptic connections of starburst amacrine cells and localization of acetylcholine receptors in primate retinas. J Comp Neurol 461:76-90.

Yoshida K, Watanabe D, Ishikane H, Tachibana M, Pastan I, Nakanishi S (2001) A key role of starburst amacrine cells in originating retinal directional selectivity and optokinetic eye movement. Neuron 30:771-780.

NOTES